Journal of Magnetic Resonance **157,** 181–189 (2002)
doi:10.1006/jmre.2002.2585

The Effects of Dissolved Oxygen upon Amide Proton Relaxation and Chemical Shift in a Perdeuterated Protein

Tobias S. Ulmer, Iain D. Campbell, and Jonathan Boyd

Department of Biochemistry, University of Oxford, Oxford OX1 3QU, United Kingdom

Received December 6, 2001; revised June 10, 2002

The effects of dissolved molecular oxygen upon amide proton ($^1H^N$) longitudinal and transverse relaxation rates and chemical shifts were studied for a small protein domain, the second type 2 module of fibronectin (^{2}F2)—isotopically enriched to 99% ^{2}H, 98% ^{15}N. Longitudinal relaxation rate enhancements, $R_{O_2}(^1H^N)$, of individual backbone $^1H^N$ nuclei varied up to 14 fold between a degassed and oxygenated (1 bar) solution, indicating that the oxygen distribution within the protein is inhomogeneous. On average, smaller relaxation rate enhancements were observed for $^1H^N$ nuclei associated with the core of the protein compared to $^1H^N$ nuclei closer to the surface, suggesting restricted oxygen accessibility to some regions. In agreement with an O_2–$^1H^N$ hyperfine interaction in the extreme narrowing limit, the $^1H^N$ transverse relaxation rates showed no significant change, up to an oxygen pressure of 9.5 bar (the maximum pressure used in this study). For most $^1H^N$ resonances, small $\Delta\delta_{O_2}(^1H^N)$ hyperfine chemical shifts could be detected between oxygen pressures of 1 bar and 9.5 bar.

Key Words: **fibronectin; hyperfine chemical shift; oxygen; paramagnetic relaxation enhancement; protein accessibility.**

INTRODUCTION

Molecular oxygen, O_2, is used as an oxidizing agent by most living organisms. Its low solubility in water explains the elaborate oxygen transport systems of complex, multicellular organisms. At 25°C and 1.013 bar (1 atm) molecular oxygen is soluble to concentrations of about 1.3 mM in water, 11.8 mM in benzene and 45.4 mM in pentane (*1*). These different solubilities reflect the apolar nature of oxygen and classify it as hydrophobic. At the cellular level, hydrophobic sites can be found within the lipid bilayer and in the core regions of globular proteins. Provided oxygen can gain access to these sites, a relatively high oxygen concentration might be anticipated there, compared to the surrounding aqueous environment. This expectation has long been verified for the lipid bilayer (*2*); further confirmation was recently provided by an NMR study which correlated the longitudinal relaxation rate enhancement, due to the dissolved oxygen, of ^{19}F nuclei with the insertion depth of the ^{19}F label (*3*). For proteins in aqueous solution, oxygen accessibility into the interior of a protein has been studied using fluorescence quenching. The fluorescence of tryptophan residues in proteins is quenched with a rate constant that is around 2–5 times slower when the side chain is in a protein compared to when it is in aqueous solution (*4*). Similarly, the rate of tyrosine quenching is slowed by about a factor of 2 between unfolded and folded protein conformations (*5*). Based on fluorescence quenching at different oxygen concentrations it was concluded that quenching is a purely dynamic, collisional process without any static, bound component (*4, 6*) and, therefore, representative of the diffusional rate of oxygen through the protein. This appears to be quite different from the defined, relatively long-lived interactions often found between water molecules and polar groups of a protein (*7*).

Solutions containing paramagnetic solutes, such as molecular oxygen, influence nuclear relaxation and nuclear energy levels of spin $-\frac{1}{2}$ nuclei through the strong local magnetic fields produced by the magnetic moment of their unpaired electron(s)—an interaction known as hyperfine coupling (*8*). There are two types of magnetic interactions between electron and nuclear spins, a dipole–dipole and scalar contact spin–spin interaction. Due to the large magnetic moment of the electron (|658| times larger than that of ^{1}H nuclear spins (*9*)) the effects of paramagnetic solutes upon the nuclear spin can often be pronounced. Oxygen-binding proteins are known to utilize either Fe^{2+} or Cu^{2+} ions to covalently bind O_2 (*10*) and we assume that for proteins without such cofactors oxygen cannot form a defined long-lived complex with the protein. In this latter case the protein–oxygen interactions are assumed to exhibit very short random lifetimes, which may vary for different sites and which are primarily governed by diffusion processes. For the dipole–dipole hyperfine interaction the nuclear and electron spins are assumed to diffuse independently and the time dependence is caused either by random variations to the interspin vector between the protein nucleus and an oxygen molecule or, in some cases, by the electron spin relaxation time (*11, 12*). If the electron *g*-tensor of the paramagnetic oxygen solute exhibits anisotropy a shift mechanism could also arise from the dipole–dipole interactions, known as the pseudo-contact shift (*8*). However, this shift will average to zero if the O_2 electron *g*-tensor does not adopt a preferred orientation with respect to a protein $^1H^N$ nucleus. In one model proposed to describe contact hyperfine interactions the molecules are considered as stuck together for a very short random time, τ_e, in which case the electron–nuclear interaction is characterized

1090-7807/02 $35.00

by a hyperfine coupling constant which is finite whenever the oxygen is stuck to the protein and is zero otherwise (*12*). The contact interaction can lead to enhanced nuclear relaxation as well as possibly changing the nuclear energy levels (*11*) and thus shifting the nuclear resonance. The contact interaction is a scalar property and is expected to fall off rapidly with an increasing number of intervening bonds between the site of delocalised spin density and the observed nucleus (*11*).

Relatively little is known about the relative efficiency of these pathways for protein–oxygen systems. In one careful study of the influence of dissolved oxygen upon the longitudinal relaxation of H_2O, it was suggested that the relaxation rate enhancement could be accounted for solely by O_2–H_2O dipole–dipole interactions without significant contributions from the contact relaxation pathway (*13*). However, hyperfine shifts between stable free radicals ("spin labels") and the solvent or cosolute molecules have been attributed mainly to contact interactions (*14*).

The present study examines the effects of dissolved molecular oxygen upon amide proton ($^1H^N$) longitudinal and transverse relaxation rates and chemical shifts for the 99% ^{2}H, 98% ^{15}N-labelled second type 2 module of fibronectin (^{2}F2) dissolved in low H_2O/D_2O solvent ratios. A recent NMR study of unlabelled ribonuclease A reported longitudinal ^{1}H relaxation rate enhancements, due to dissolved oxygen (*15*). By working in a highly deuterated environment very much reduced longitudinal relaxation rates can be expected compared to an unlabelled protein. This makes the small rate enhancements from the oxygen solute easier to detect and reduces the mutual averaging of spin magnetisation, through spin diffusion (*16*). Longitudinal relaxation rate enhancements of individual backbone $^1H^N$ nuclei varied up to 14-fold between a degassed and oxygenated (1 bar) solution. The $^1H^N$ transverse relaxation rates showed no significant change, up to an oxygen pressure of 9.5 bar (the maximum pressure used in this study). For most $^1H^N$ resonances, small O_2–$^1H^N$ hyperfine chemical shifts could be detected between oxygen pressures of 1 bar and 9.5 bar.

MATERIALS AND METHODS

Protein Production and NMR Sample Preparation

The 59-residue second type 2 module of human fibronectin (^{2}F2), residues 375 to 433, was produced by recombinant expression from the methylotrophic yeast *P. pastoris* as described (*17*). Isotopic labelling was achieved by using >99% ^{2}H enriched reagents and >98% ^{15}N enriched $(ND_4)_2SO_4$. Two NMR samples were prepared [1]. Freeze-dried protein was dissolved in 10%/90% H_2O/D_2O to ~2 mM and the pH[1] was adjusted to 4.0. The sample was degassed by three freeze–pump–thaw cycles in the NMR tube (Wilmad 542-PP-8) with subsequent flame sealing of the tube. Oxygenation of sample [1] to ~1.0 bar was achieved after opening the tube by bubbling the degassed sample for 10 min with oxygen (BOC gases U.K., zero-grade oxygen 100%) at 5°C. The pH of the sample remained constant to within ±0.05 units (the accuracy of the measurement). [2] Freeze-dried protein was dissolved in 30%/70% H_2O/D_2O to ~1.5 mM and the pH was adjusted to 4.0. Oxygenation of this sample to 5.5 or 9.5 bar in a Wilmad 524-PV-7 NMR tube was achieved by pressurizing with oxygen after carefully purging the air from the system and finally sealing the tube using the supplied Teflon valve. The ^{1}H longitudinal relaxation time of the bulk solvent was used to monitor the slow dissolution of the oxygen gas into this protein solution. At 25°C about 4 days and at 5°C about 6 days, respectively, were required for the ^{1}H T_1 of the bulk solvent to reach a constant value. The T_1 of the bulk solvent was monitored throughout these experiments and once the sample had equilibrated no change was observed to the ^{1}H T_1 of the solvent during a series of experiments.

Measurement of $^1H^N$ Longitudinal Relaxation

Measurements for sample [1] were performed at 5°C and at a ^{1}H frequency of 750 MHz. ^{1}H longitudinal relaxation was followed by one-dimensional, nonselective inversion–recovery experiments as described by Freeman and Hill (*18*). In this approach, the $^1H^N$ longitudinal magnetizations $H_z^N(t)$ and $H_z^N(\infty)$ are acquired on alternate scans and subtracted so that the difference magnetization is collected directly. $^1H^N$ and ^{15}N assignments were obtained from HSQC spectra (*19*) and the known ^{2}F2 shifts (*17*). A very high signal-to-noise 1D ^{1}H spectrum showed no detectable broad peaks from exchangeable side chain protons near the backbone $^1H^N$ resonances (data not shown). Seventeen relaxation delays ranging from 0.16 s to 20.8 s and a recycle delay of 100 s were used. The solvent magnetization was placed at $+I_z$ at the start of the relaxation delay using a Gaussian shaped pulse (*20*) of 2 ms duration. Chemical shift anisotropy (CSA)-dipolar cross-correlation phenomena was removed by the application of 180° ^{15}N pulses every 80 ms (*21*). Data were processed with Felix 2.3 (Biosym Inc., San Diego, CA). Peak intensity data were fitted with a two-parameter monoexponential model, $I(t) = A * \exp(-R_1 t)$, to extract the relaxation rate $R_1 = 1/T_1$. Uncertainties in peak intensities were determined from duplicate datasets. Monte Carlo simulations were performed to estimate errors.

The disadvantage of the Freeman and Hill approach, of having to wait $5T_1$ between scans, is compensated by high accuracy; however, it renders a two-dimensional version impractical due to the long $^1H^N$ T_1 relaxation times. A two-dimensional saturation-recovery HSQC-detected experiment (*22*), which avoids the $5T_1$ relaxation recovery period, exhibited two to threefold larger uncertainties and the initial magnetization state of the solvent proved more difficult to control.

Longitudinal Relaxation Times of the Bulk Solvent

Solvent chemical exchange processes are an important contributor to $^1H^N$ longitudinal relaxation and, therefore, we report the observed ^{1}H T_1 relaxation times at 750 MHz for the bulk

solvent in each sample. For sample [1] degassed, 5°C and with radiation damping suppressed (*23*) ^{1}H $T_1 = 8.9$ s. After bubbling with oxygen for 10 min the ^{1}H T_1 was reduced to 1.82 s. For sample [2] 25°C after equilibration (see above) in the presence of 9.5, 5.5, and 1 bar of oxygen the ^{1}H T_1 relaxation times of the solvent were 0.50 s, 0.93 s, and 3.0 s respectively.

Measurement of $^1H^N$ Transverse Relaxation

Measurements using sample [2] were performed at 750 MHz employing the pulse sequence described by Ishima *et al.* (*24*) with $^1H^N$ relaxing as unlike spins during a Carr–Purcell–Meiboom–Gill (CPMG) echo sequence. Eight relaxation delays ranging from 6.7 to 134.3 ms were used at 5°C. A recycle delay of 10 s, a CPMG delay of 400 μs, and a B_1 field strength of 28.1 kHz were used. Radiation damping of the solvent was suppressed by the application of weak gradient pulses during the relaxation period (*23*). Chemical shift anisotropy (CSA) and dipolar cross-correlation was removed by application of nitrogen 180° pulses in the middle of the basic CPMG block (*25, 26*). Peak intensity data were fitted with the two-parameter monoexponential model to extract the transverse relaxation rate $R_2 = 1/T_2$. Monte Carlo simulations were performed to estimate errors.

Measurement of Oxygen-Induced $^1H^N$ Shifts

The $^1H^N$ chemical shifts of sample [2] were measured at 25°C and 750 MHz using a cycle of oxygen pressures of 1–5.5–9.5–1 bar (BOC gases U.K., zero-grade oxygen 100%). $^1H^N$ shift information was obtained either from 2D TROSY-HSQC spectra (*27, 28*) or from 1D ^{1}H spectra. For each spectrum 8192 complex points (per increment) were recorded with an acquisition time of 655.4 ms (in the ^{1}H dimension). After a Lorentzian-to-Gaussian resolution enhancement, the FIDs were zero-filled to 65,536 points to give a final digital resolution of 0.19 Hz (in the ^{1}H dimension). Peak picking was accomplished with Felix 2.3 (Biosym Inc., San Diego, CA, U.S.A.). The $^1H^N$ shift changes could be reproduced, upon repetition of the pO_2 1–5.5–9.5–1 bar cycle, to within the digital resolution. The effects of pressure on the $^1H^N$ shifts, within the range of 1 to 9.5 bar, was assessed using N_2 (BOC gases U.K., oxygen-free nitrogen) in place of O_2.

RESULTS AND DISCUSSION

Effects of Dissolved Oxygen on $^1H^N$ Longitudinal Relaxation

The quadratic dependence of paramagnetic relaxation on the magnetogyric ratio, γ, of the nuclear spin (*8*) makes the ^{1}H nucleus particularly sensitive to effects from paramagnetic substances, such as dissolved oxygen. However, in proteins ^{1}H is also the most abundant nucleus, which leads to very many ^{1}H–^{1}H dipolar interactions that reduce the relative contribution of paramagnetic relaxation to the overall relaxation. Moreover, proton longitudinal relaxation is often dominated by cross-relaxation between neighboring ^{1}H spins, which leads to extensive exchange of spin magnetization and to the relay of spin magnetization over several spins (spin diffusion) (*16*). The resulting relatively uniform, fast longitudinal relaxation characteristics of all the protein ^{1}H spins (*16*) limit the information content of individual rate constants. These adverse effects can be greatly reduced by replacing all nonlabile (carbon-bonded) protons with deuterons by diluting the labile (nitrogen- and oxygen-bonded) protons with low H_2O/D_2O ratios and then studying the residual backbone amide protons ($^1H^N$). Dipolar interactions will then be restricted to conformation-dependent, interresidue $^1H^N$–$^1H^{N,O}$ interactions and intraresidue $^1H^N$–^{15}N interactions and there will be numerous weak $^1H^N$–$^2H^{N,O,C}$ interactions. In this highly deuterated environment, the small effect of dissolved oxygen on proton relaxation is thus easier to observe and the high dilution of ^{1}H spins renders the relay of spin magnetization (spin diffusion) between ^{1}H spins relatively inefficient.

In the absence of efficient spin diffusion, cross-relaxation between dipolar coupled spins falls off with an r^{-6} distance dependence (*29*). Any ensuing exchange of spin magnetization of a particular $^1H^N$ nucleus is therefore restricted to neighboring ^{1}H nuclei within about 5–7 Å (*30*). Upon oxygenation of the sample solution a paramagnetic contribution, R_{O_2}, is introduced to the self-relaxation of the spins while the cross-relaxation is left unchanged. Within these assumptions the longitudinal paramagnetic relaxation contribution at a particular $^1H^N$ site, $R_{O_2}(^1H^N)$, has been measured as the difference of the $^1H^N$ longitudinal relaxation recoveries in degassed and oxygenated solution. Figure 1 shows two examples from the small ^{2}F2 protein module (*17*), W40 and T5, having slow and fast $^1H^N$ longitudinal relaxation characteristics. Figure 2a shows all of the measured $R_{O_2}(^1H^N)$ rate enhancements in the presence of ~1.9 mM dissolved oxygen, which is the concentration expected at ~1.0 bar O_2 and 5°C (*1*). The relaxation enhancements vary greatly between different amide proton sites—by up to a factor of ~14 (for G33 and G42). Figures 2b and 2c shows the measured longitudinal relaxation rate enhancements, $R_{O_2}(^1H^N)$, mapped onto the average ^{2}F2 solution structure.

It is expected that for the diffusion model of dipole–dipole electron–nuclear interactions the dominant contributions to nuclear relaxation come from the translational diffusion correlation time determined by the relative translational diffusion constants of the protein and oxygen molecules, the distance of closest approach, d, of a $^1H^N$ nucleus and an oxygen molecule and the local oxygen concentration surrounding the $^1H^N$ nucleus. The dipolar interaction will also be influenced by the electron spin longitudinal relaxation time, T_{1e}, when this is faster than the translational diffusion correlation time (*8, 14*), i.e., if the electron spin changes its orientation before the protein–oxygen orientation changes. Nuclear relaxation depends upon the intensity of the spectral densities at $J(\omega_H)$ and $J(\omega_E)$ and these depend upon the correlation time for the hyperfine interaction (*14*). Dissolved oxygen is known to have a relatively fast electron spin longitudinal relaxation time, T_{1e}, of ~7.5 ps in solution (*31*), and this value of ~7.5 ps has been measured in several different solvents which

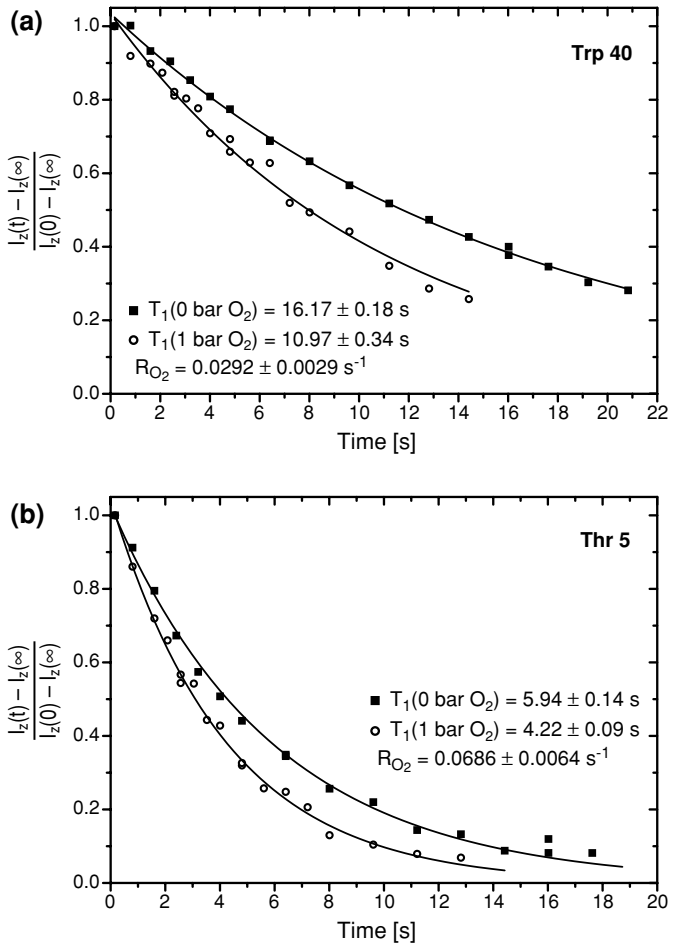

FIG. 1. $^1H^N$ longitudinal relaxation decays of (a) Trp40 and (b) Thr5 in a degassed and oxygenated solution of 2 mM 99% ^2H, 98% ^{15}N-labelled $^2F2$ in 10%/90% H_2O/D_2O, pH 4.0 (sample [1]) at 5°C and 750 MHz. The solvent magnetization was set to $+I_z$ prior to the relaxation delay in nonselective inversion–recovery experiments. In the oxygenated solution an oxygen concentration of ~1.9 mM can be expected (~1.0 bar O_2 at 5°C (*1*)). Monoexponential fits, $I(t) = A * \exp(-R_1 t)$, to the data are shown. The difference between the apparent relaxation rates, $R_1 = 1/T_1$, in the degassed and oxygenated solutions, $R_{O_2}(^1H^N)$, is quoted. For the present system, we note that the longitudinal relaxation decays agree well with monoexponential fits.

can be assumed to give some reflection of the different chemical environments for oxygen found in proteins. The diffusional correlation time, τ_d, is estimated at ~330 ps (calculated using $\tau_d = 2d^2/(D_p + D_{O_2})$ (*14*) with $d = 2.72$ Å and using values for the self-diffusion coefficients in 10%/90% H_2O/D_2O at 5°C of $D_p = 5 * 10^{-11} m^2 s^{-1}$ and $D_{O_2} = 40 * 10^{-11} m^2 s^{-1}$). The $^2F2$ isotropic rotational correlation time, τ_r, is estimated to be ~7 ns. Assuming the effective correlation time for the electron–nuclear dipolar coupling can be written as $1/\tau = 1/T_{1e} + 1/\tau_d + 1/\tau_r$ (*8*) the dominant correlation time is most likely T_{1e}. Furthermore, fluorescence quenching has suggested that the diffusion of oxygen within proteins is slower than when free in solution (*4, 5*) supporting the hypothesis that the dominant correlation time for the dipolar interaction is most likely T_{1e}. In the case where no binding site exists and the O_2–$^1H^N$ dipolar interaction is determined by motions characterized by T_{1e} the dipolar contribution, $R_1(O_2^d)$, to the experimental $R_{O_2}(^1H^N)$ rate enhancement for a fully accessible nucleus can be estimated using the equation (*14*)

$$R_1(O_2^d) = (8\pi/45)(\mu_0/4\pi)^2 N_A C \gamma_H^2 g_e^2 \mu_\beta^2 S(S+1) \times \{3T_{1e}/(1+\omega_H^2 T_{1e}^2) + 7T_{2e}/(1+\omega_e^2 T_{2e}^2)\}/d^3, \quad [1]$$

where N_A is Avogadro's constant, C is the concentration of molecular oxygen, and other symbols have their usual meaning (*14*). Inserting values for $C = 1.9$ mol m^{-3}, $d = 2.72$ Å, $T_{1e} = 7.5 * 10^{-12}$ s, $S = 1$, $\omega_H = 2\pi * 750 * 10^6$ rad s^{-1}, and neglecting a small contribution from the spectral density involving T_{2e}, $R_1(O_2^d) = 0.35$ s^{-1}. The average value for the experimental rate enhancements, $R_{O_2}(^1H^N)$, was found to be 0.11 ± 0.07 s^{-1} (Fig. 2a). Thus, it seems reasonable to adopt this model for the dipolar interaction with variations in the rate enhancement, $R_{O_2}(^1H^N)$, being caused primarily by variations in the local concentration of molecular oxygen, C, and the distance of closest approach, d, and to a lesser extent by variations in the electron spin correlation time, T_{1e}, caused by different environments. In analogy to the O_2–H_2O system (*13*), the contact contribution to the rate enhancements is probably relatively small. Although in order to quantitatively distinguish the relative contributions from the dipolar and scalar relaxation processes to the overall rate enhancements it is first necessary to propose a model for the scalar interactions (*12*).

The $R_{O_2}(^1H^N)$ rate enhancements appear, on average, lower for residues associated with the protein interior (Y26, W40, G42, F53) than for residues close to the surface (N4, G7, G12, G33, A59) (Fig. 2). Such a trend is in agreement with the results from a previous NMR study of unlabelled ribonuclease A (*15*). From polarity arguments, this is not the expected result, as higher oxygen concentrations are found in phospholipids and apolar liquids than in water. A central quantity in theories of hydrophobic solubilities is the energy required to open, in the solvent, a cavity of size sufficient to accommodate the solute (*32–34*). In comparison to liquid systems, functional groups within the core regions of proteins have a defined structural relationship with each other. The creation of cavities within the protein interior to accommodate oxygen (i.e., the access of oxygen into the protein interior) therefore appears to be relatively unfavorable. This suggests that one factor determining the solubility of oxygen in a globular protein is determined by space restraints rather than polarity differences.

Some features in the distribution of $R_{O_2}(^1H^N)$ rates are highlighted. Given the large differences in O_2 solubility between polar and apolar solvents (see Introduction), some $^1H^N$ sites may be able to dissolve more oxygen than the aqueous solvent. $^2F2$ carries a GlnNAc carbohydrate unit N-linked to Asn25 (*17*), providing one solvent-exposed $^1H^N$ nucleus from each side chain (Fig. 2b and c) that appears suited to serve as a reference for fully

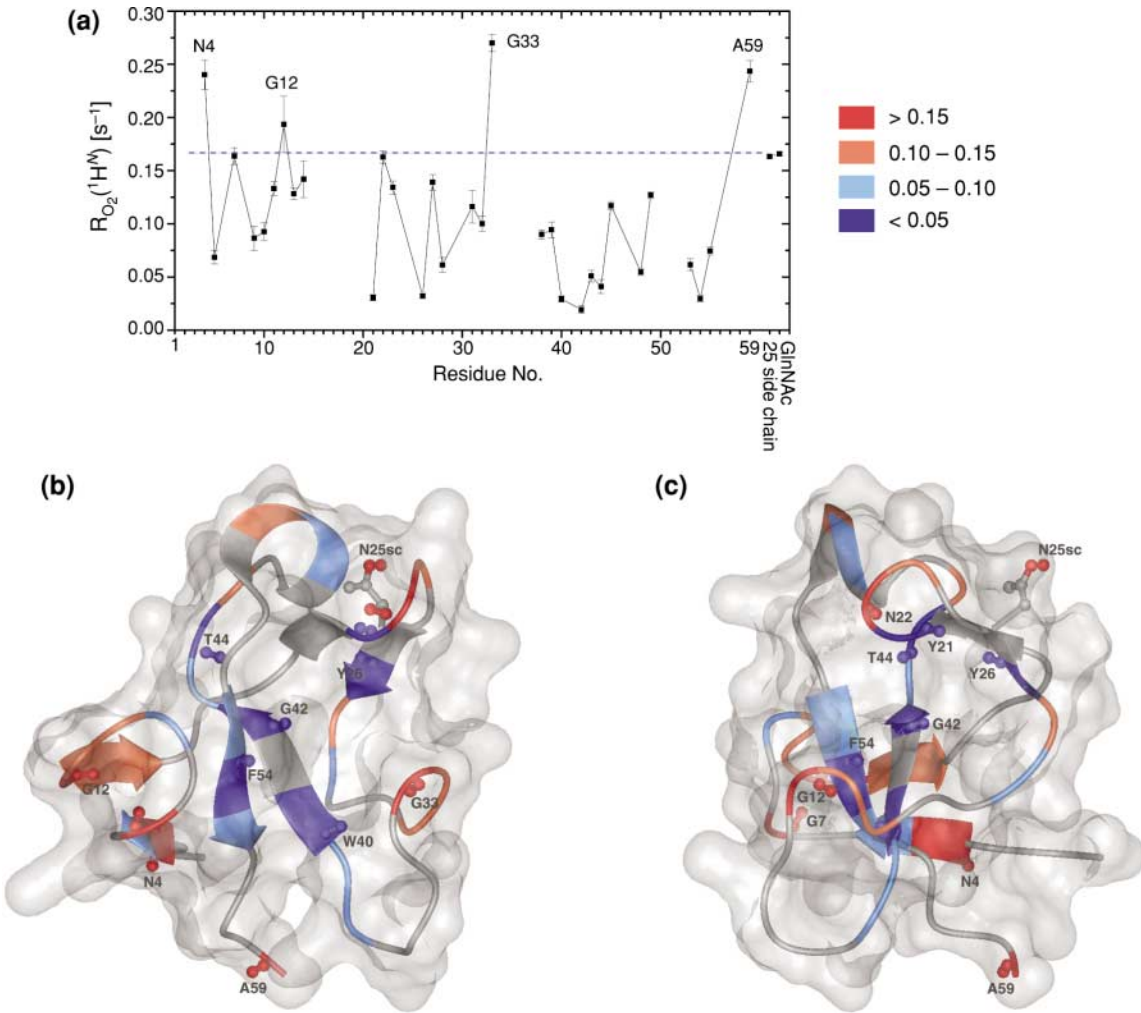

FIG. 2. (a) Longitudinal relaxation rate enhancements, $R_{O_2}(^1H^N, \sim 1.9$ mM $O_2)$, as a function of residue number. Rate enhancements were obtained for 31 out of 56 backbone amides using a one-dimensional, nonselective inversion–recovery approach. Two more $R_{O_2}(^1H^N)$ rates were obtained. One for the $^1H^N$ nucleus of the side chain of Asn25, which carries a GlnNAc carbohydrate unit that possesses the second $^1H^N$ nucleus (*17*). These two rate enhancements, which are very similar, are taken as an estimate for fully solvated $^1H^N$ nuclei. (b) $R_{O_2}(^1H^N, \sim 1.9$ mM $O_2)$ rates mapped color-coded onto the backbone representation of the backbone ^{2}F2 average solution structure (*17*). For selected residues the N–H atoms are shown colour-coded, too. Residues for which no data could be obtained are shown in grey. The Asn25 side chain is shown in grey. The GlnNAc carbohydrate unit is not shown. The van der Waals contact surface is drawn transparently. (c) A 90° z-axis rotated view of (b). Figure generated with MOLMOL (*42*).

solvent exposed $^1H^N$ sites (Fig. 2a). Four backbone $^1H^N$ nuclei (N4, G12, G33, A59) are found to have even larger $R_{O_2}(^1H^N)$ rate enhancements than those from the side chains of Asn25 and GlnNAc possibly indicating these sites are in a relatively accessible hydrophobic environments. Interestingly, all of these residues are relatively close to the surface (Fig. 2b and c). The C-terminal residue, A59, is also known to exhibit extensive internal mobility (*35*).

Extensive mutagenesis studies of the Fe-containing oxygen-binding site of hemerythrin has suggested that a highly conserved (hydrophobic) leucine residue near the oxygen-binding site is important in keeping the solvent *away* from the binding site rather than for gating O_2 *into* the binding site (*36, 37*). Drawing upon these authors' conclusions it is possible that intimate $^1H^N$–H_2O contacts explain some of the relatively low $R_{O_2}(^1H^N)$ rate enhancements for residues close to the surface. A more quantitative discussion and description of the polarity and accessible volume of each amide proton microenvironment would be desirable. However, such a treatment is beyond the current study. For example, for all but a few $^1H^N$ nuclei of ^{2}F2 the calculated solvent accessible surface area is zero (*38*), which does not correlate with the $R_{O_2}(^1H^N)$ rate enhancements.

Effects of Dissolved Oxygen on $^1H^N$ Transverse Relaxation

In the limit of a very short electron–nuclear correlation time ("extreme narrowing limit"), relaxation contributions to the $^1H^N$ transverse relaxation rate, $R_2(^1H^N)$, from $^1H^N$–O_2

dipole–dipole and contact interactions are expected to be essentially the same as for the $^1H^N$ longitudinal relaxation rates (*9*). $R_2(^1H^N)$ can, therefore, serve as a measure of the timescale of the correlation time for the O_2–$^1H^N$ electronic-nuclear coupling within the protein.

The average $^1H^N$ longitudinal relaxation rate enhancement due to the ~1.9 mM dissolved oxygen at 1 bar is $0.11 \pm 0.07\ s^{-1}$ and compared to typical $^1H^N$ transverse relaxation rates found in proteins this is relatively small. Hence, we have measured the transverse relaxation at oxygen pressures of ~1 and ~9.5 bar corresponding to dissolved oxygen concentrations of ~1.9 mM and ~18.2 mM, respectively, at 5°C (*1*). Employing identical assumptions to those used above for the discussion of the longitudinal rate enhancements, the dipolar contribution, $R_2(O_2^d)$, to the transverse relaxation rate enhancements, at 9.5 bar, can be obtained via the relationship

$$R_2\left(O_2^d\right) = 7/6 R_1^{av}\left(O_2^d\right) C_{9.5}/C_1, \qquad [2]$$

where $C_{9.5}/C_1$ is the ratio of oxygen concentrations at the two pressures (*14*). Hence, at ~9.5 bar the additional dipolar contribution to the transverse relaxation rate enhancement is only $\sim 1\ s^{-1}$. The average $R_2(^1H^N)$ relaxation rate at ~1 bar O_2 and 5°C was found to be $12.5\ s^{-1}$ in 30%/70% H_2O/D_2O (Fig. 3) and no significant $R_2(^1H^N)$ relaxation rate differences were detected between the samples at 1 and 9.5 bar O_2 (Fig. 3). These data support the idea that the O_2–$^1H^N$ electron–nuclear coupling, within the protein environment, is in the extreme narrowing limit. There is a further possible relaxation contribution, from the interaction of the nuclear magnetic moments with the bulk static magnetic moment, arising from the population difference of the electron spins (Curie spin relaxation) (*8*). This interaction is governed by the rotational correlation time of the protein, and, hence, would affect transverse relaxation in proteins much more than longitudinal relaxation. From the data presented here, this contribution appears to be small.

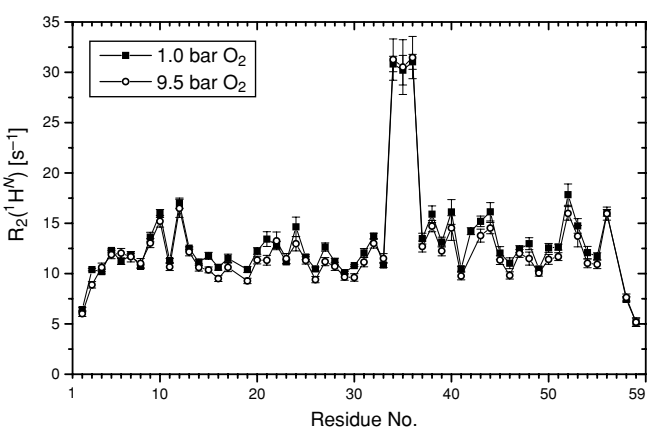

FIG. 3. $^1H^N$ transverse relaxation rates of 1.5 mM 99% ^2H, 98% ^{15}N labelled $^2F2$ in 50 mM acetic-d_3 acid, 30%/70% H_2O/D_2O, pH 4.0 (sample [2]) at 5°C and 750 MHz. Oxygen pressures of 1 and 9.5 bar were employed. No significant differences could be detected.

It is worth noting that the property of considerably shortening longitudinal relaxation, while not significantly affecting transverse relaxation, makes elevated concentrations of molecular oxygen potentially useful for reducing the recycle delay in NMR experiments when using samples with high deuteration levels and/or at very high magnetic fields (*39*).

Effects of Dissolved Oxygen on $^1H^N$ Chemical Shift

The observed $^1H^N$ paramagnetic longitudinal relaxation enhancements demonstrate a hyperfine interaction between the unpaired oxygen electrons and the $^1H^N$ protein nuclei. As a result, a $^1H^N$ hyperfine shift may be present. Small, primarily upfield (low frequency), oxygen induced ^1H shift changes have previously been reported for small organic molecules in CCl_4 solution (*40*). In this study, small $\Delta\delta_{O_2}(^1H^N)$ shift differences between the different oxygen pressures were observed for most $^1H^N$ protein resonances (Fig. 4). At the moderate oxygen pressure difference of ~8.5 bar (~9.5 vs. 1.0 bar), small upfield (low frequency) and downfield (high frequency) $\Delta\delta_{O_2}(^1H^N)$ shift differences up to a maximum of about −1.5 Hz and +0.9 Hz, respectively, were found at 750 MHz. A few $^1H^N$ resonances exhibited no apparent detectable change to their chemical shifts within the pressure range studied (Fig. 4b). Interestingly, the ^1H resonances from traces of the small organic cosolutes citrate and acetate exhibit much larger downfield shifts of +6.1 Hz (Fig. 4b).

In the present system, a $\Delta\delta_{O_2}(^1H^N)$ shift change between two different concentrations of dissolved oxygen could have contributions from a hyperfine shift, δ_{hf}, but also from changes in protein structure due to the increased pressure, δ_{str}, and from a change in the bulk magnetic susceptibility of the sample, δ_χ. To assess the shift change due to the effects of pressure, N_2, which is diamagnetic and apolar, like O_2 (*1*), was used in place of O_2. No significant shift changes could be detected in either the protein $^1H^N$ resonances or to the ^1H resonances from the small molecule impurities (data not shown). This result is not unexpected, as studies of proteins at pressures up to 2,000 bar (*41*) have shown only quite small $^1H^N$ shift changes of on average ~0.028 Hz/bar. This is equivalent to ~0.24 Hz for a pressure difference of 8.5 bar, which is lower than some of the measured $\Delta\delta_{O_2}(^1H^N)$ shift differences and is estimated to be close to the detection limit of the measurements reported here. The difference in oxygen concentration between 9.5 and 1 bar oxygen is estimated to be ~11 mM at 25°C (*1*). As a consequence, the bulk magnetic susceptibility of the sample solution will increase giving rise to a uniform downfield shift (higher frequency) for all resonances. However, assuming that the ^2H in the resonance of the D_2O, used by the field frequency lock, is equally affected by the increased bulk sample paramagnetism, the lock should compensate for this uniform shift difference and maintain a similar magnetic field strength at each oxygen pressure. However, if the ^2H nucleus experiences in addition a small contact shift at the

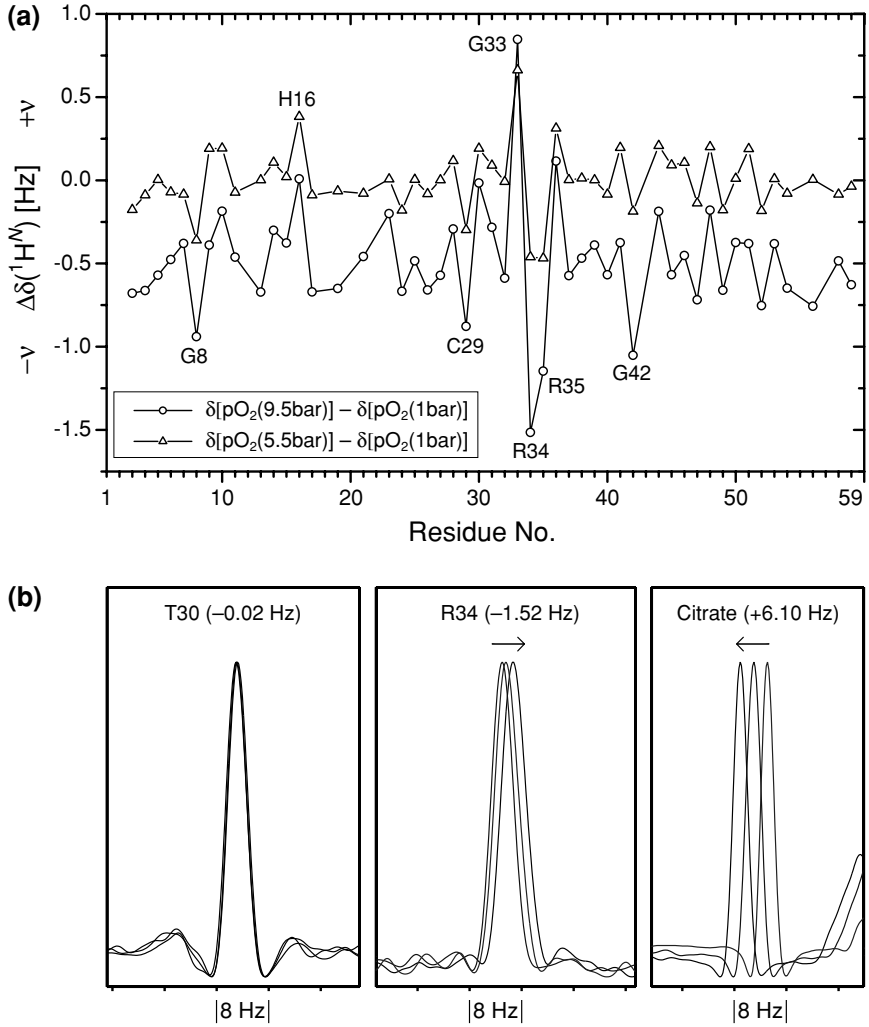

FIG. 4. (a) The $\Delta\delta_{O_2}(^1H^N)$ shift differences observed between ^{2}F2 solutions (sample [2]) oxygenated to (1 and 5.5) and (1 and 9.5) bar at 25°C and 750 MHz. (b) $^1H^N$ cross sections for T30, R34 from $^1H^N$–^{15}N TROSY-HSQC spectra and $^1H^C$ sections for citrate from 1D ^{1}H spectra. Peak intensities were normalized. The origin of the frequency axis is chosen arbitrarily for each panel. Relative shift changes between the 1 and 9.5 bar datasets are quoted in the figure.

larger O_2 pressure then the B_0 field strength will not be the same at each oxygen pressure, having the effect of introducing a constant shift into the $\Delta\delta_{O_2}(^1H^N)$ values. The nonuniformity of the shift differences, both upfield and downfield, demonstrate that the observed oxygen-dependent $\Delta\delta_{O_2}(^1H^N)$ values arise predominantly from a hyperfine interaction. However, a small uniform offset does become apparent between the (9.5–1 bar) and (4.5–1 bar) $\Delta\delta_{O_2}(^1H^N)$ shift differences, Fig. 4a.

The hyperfine shift, δ_{hf}, is commonly factorized into two terms, a contact and pseudo-contact term (δ_{con} and δ_{mc}), which are related to the contact and dipolar relaxation pathways, respectively. A pseudo-contact (dipolar) shift, δ_{mc}, is orientation dependent and in the absence of a specific O_2 binding site defined $^1H^N$–O_2 orientations would require an alignment of O_2 within the protein framework presumably caused by steric or electrostatic effects. A contact shift possesses no such geometric requirement and the delocalisation of unpaired electron density near or at a $^1H^N$ nucleus in a protein is conceivable either upon close approach or when the molecules are stuck together for a random period (*12*).

The small molecules acetate and citrate are found to exhibit much larger $\Delta\delta_{O_2}(^1H^C)$ shift differences than observed for the protein $^1H^N$ nuclei. In analogy to the fluorescence quenching studies of free tryptophan vs tryptophan residues in proteins (*4*), the small organic molecules are less shielded from collisions with oxygen than the protein $^1H^N$ nuclei. It is found that the $\Delta\delta_{O_2}(^1H^N)$ shift differences do not correlate well with the longitudinal relaxation rate enhancements, $R_{O_2}(^1H^N)$ (correlation coefficient $R = -0.38$). The lack of a significant correlation indicates that that the processes causing the $\Delta\delta_{O_2}(^1H^N)$ shift differences and the $R_{O_2}(^1H^N)$ rate enhancements are different. It appears most plausible that the chemical shift differences are

caused mainly by contact interactions whereas the $R_{O_2}(^1H^N)$ rate enhancements are dominated by dipole–dipole interactions. The observation of contact shifts would, however, imply some contact contribution to the $R_{O_2}(^1H^N)$ rate enhancements. For those seven residues exhibiting the most prominent upfield or downfield shift changes (G8, H16, C29, G33, R34, R35, G42—see Fig. 4a) obvious dynamic or structural peculiarities can be identified for only three of them. R34 and R35 are in a region that is not very well defined in the solution structure of ^{2}F2 (*17*) and is somewhat more mobile than the remainder of the protein backbone, as judged from their ^{15}N–$\{^1H\}$ heteronuclear NOEs. The $^1H^N$ nucleus of G42 exhibits a chemical shift of 3.49 ppm indicative of the formation of an aromatic hydrogen bond with the benzene ring of the adjacent F19 (*17*). This suggests that relatively subtle differences between individual O_2–$^1H^N$ interactions can lead to relatively big variations of the contact term.

ACKNOWLEDGMENTS

We thank Andy Pickford and Ulrich Schwarz-Linek for help with protein production and purification. T.S.U. acknowledges support from BBSRC. I.D.C. acknowledges support from the Wellcome Trust. The Oxford Centre for Molecular Sciences is funded by MRC, BBSRC, and EPSRC.

REFERENCES

1. P. G. T. Fogg and W. Gerrard, "Solubility of Gases in Liquids," Wiley, Chichester (1991).
2. D. A. Windrem and W. Z. Plachy, The diffusion-solubility of oxygen in lipid bilayers, *Biochim. Biophys. Acta* **600,** 655–665 (1980).
3. R. S. Prosser, P. A. Luchette, and P. W. Westerman, Using O-2 to probe membrane immersion depth by F-19 NMR, *Proc. Natl. Acad. Sci. U.S.A.* **97,** 9967–9971 (2000).
4. J. R. Lakowicz and G. Weber, Quenching of protein fluorescence by oxygen: Detection of structural fluctuations in proteins on the nanosecond time scale, *Biochemistry* **12,** 4171–4179 (1973).
5. J. R. Lakowicz and P. M. B., Oxygen quenching and fluorescence depolarization of tyrosine residues in proteins, *J. Biol. Chem.* **258,** 4794–4801 (1983).
6. J. R. Lakowicz and G. Weber, Quenching of fluorescence by oxygen: A probe for structural fluctuations in macromolecules, *Biochemistry* **12,** 4161–4170 (1973).
7. G. Wider, R. Riek, and K. Wuthrich, Diffusion filters for separation of solvent-protein and protein-protein nuclear overhauser effects (HYDRA), *J. Am. Chem. Soc.* **118,** 11,629–11,634 (1996).
8. L. Banci, I. Bertini, and C. Luchinat, "Nuclear and Electron Relaxation," VCH, Weinheim (1991).
9. I. Bertini, C. Luchinat, and S. Aime, NMR of paramagnetic substances, *Coord. Chem. Rev.* **150,** 1–300 (1996).
10. D. M. Kurtz, Oxygen-carrying proteins: Three solutions to a common problem, *Essays in Biochem.* **34,** 85–100 (1999).
11. N. Bloembergen, Proton relaxation times in paramagnetic solutions, *J. Chem. Phys.* **27,** 572–573 (1957).
12. P. S. Hubbard, Theory of electron-nucleus Overhauser effects in liquids containing free radicals, *Proc. Roy. Soc. A* **291,** 537–555 (1966).
13. R. Hausser and F. Noack, Kernmagnetische relaxation und korrelation im system Wasser-Sauerstoff, *Z. Naturforsch. A* **20,** 1668–1675 (1965).
14. I. Bertini and C. Luchinat, "NMR of Paramagnetic Molecules in Biological Systems," Benjamin/Cummings, Menlo Park, CA (1986).
15. C. L. Teng and R. G. Bryant, Experimental measurement of nonuniform dioxygen accessibility to ribonuclease a surface and interior, *J. Am. Chem. Soc.* **122,** 2667–2668 (2000).
16. A. Kalk and H. J. C. Berendsen, Proton magnetic relaxation and spin diffusion in proteins, *J. Magn. Reson.* **24,** 343–366 (1976).
17. H. Sticht, A. R. Pickford, J. R. Potts, and I. D. Campbell, Solution structure of the glycosylated second type 2 module of fibronectin, *J. Mol. Biol.* **276,** 177–187 (1998).
18. R. Freeman and H. D. W. Hill, Fourier transform study of NMR spin-lattice relaxation by "progressive saturation," *J. Chem. Phys.* **54,** 3367–3377 (1971).
19. J. Boyd, N. Soffe, B. John, D. Plant, and R. Hurd, The generation of phase-sensitive 2*d* N-15-H-1 spectra using gradient pulses for coherence-transfer-pathway selection, *J. Magn. Reson.* **98,** 660–664 (1992).
20. C. Bauer, R. Freeman, T. Frenkiel, J. Keeler, and A. J. Shaka, Gaussian pulses, *J. Magn. Reson.* **58,** 442–457 (1984).
21. J. Boyd, U. Hommel, and I. D. Campbell, Influence of cross-correlation between dipolar and anisotropic chemical-shift relaxation mechanisms upon longitudinal relaxation rates of N-15 in macromolecules, *Chem. Phys. Lett.* **175,** 477–482 (1990).
22. T. Yamazaki, W. Lee, C. H. Arrowsmith, D. R. Muhandiram, and L. E. Kay, A suite of triple-resonance NMR experiments for the backbone assignment of N-15, C-13, H-2 labeled proteins with high-sensitivity, *J. Am. Chem. Soc.* **116,** 11,655–11,666 (1994).
23. V. Sklenar, Suppression of radiation damping in multidimensional NMR experiments using magnetic-field gradients, *J. Magn. Reson. Ser. A* **114,** 132–135 (1995).
24. R. Ishima, P. T. Wingfield, S. J. Stahl, J. D. Kaufman, and D. A. Torchia, Using amide H-1 and N-15 transverse relaxation to detect millisecond time-scale motions in perdeuterated proteins: Application to HIV-1 protease, *J. Am. Chem. Soc.* **120,** 10,534–10,542 (1998).
25. A. G. Palmer, N. J. Skelton, W. J. Chazin, P. E. Wright, and M. Rance, Suppression of the effects of cross-correlation between dipolar and anisotropic chemical-shift relaxation mechanisms in the measurement of spin–spin relaxation rates, *Mol. Phys.* **75,** 699–711 (1992).
26. J. Boyd, U.Hommel, and V. V. Krishnan, Influence of cross-correlation between dipolar and chemical-shift anisotropy relaxation mechanisms upon the transverse relaxation rates of N-15 in macromolecules, *Chem. Phys. Lett.* **187,** 317–324 (1991).
27. K. Pervushin, R. Riek, G. Wider, and K. Wuthrich, Attenuated T-2 relaxation by mutual cancellation of dipole-dipole coupling and chemical shift anisotropy indicates an avenue to NMR structures of very large biological macromolecules in solution, *Proc. Natl. Acad. Sci. U.S.A.* **94,** 12,366–12,371 (1997).
28. T. Schulte-Herbruggen and O. W. Sorensen, Clean TROSY: Compensation for relaxation-induced artifacts, *J. Magn. Reson.* **144,** 123–128 (2000).
29. I. Solomon, Relaxation processes in a system of two spins, *Phys. Rev.* **99,** 559–565 (1955).
30. T. K. Mal, S. J. Matthews, H. Kovacs, I. D. Campbell, and J. Boyd, Some NMR experiments and a structure determination employing a {N-15,H-2} enriched protein, *J. Biomol. NMR* **12,** 259–276 (1998).
31. C. L. Teng, H. Hong, S. Kiihne, and R. G. Bryant, Molecular oxygen spin-lattice relaxation in solutions measured by proton magnetic relaxation dispersion, *J. Magn. Reson.* **148,** 31–34 (2001).
32. G. L. Pollack, Why gases dissolve in liquids, *Science* **251,** 1323–1330 (1991).

33. L. R. Pratt and A. Pohorille, Theory of hydrophobicity—Transient cavities in molecular liquids, *Proc. Natl. Acad. Sci. U.S.A.* **89,** 2995–2999 (1992).

34. G. Hummer, S. Garde, A. E. Garcia, and L. R. Pratt, New perspectives on hydrophobic effects, *Chem. Phys.* **258,** 349–370 (2000).

35. S. P. Smith, Y. Hashimoto, A. R. Pickford, I. D. Campbell, and J. M. Werner, Interface characterization of the type II module pair from fibronectin, *Biochemistry* **39,** 8374–8381 (2000).

36. C. S. Farmer, D. M. Kurtz, R. S. Phillips, J. Y. Ai, and J. Sanders-Loehr, A leucine residue "gates" solvent but not O-2 access to the binding pocket of Phascolopsis gouldii hemerythrin, *J. Biol. Chem.* **275,** 17043–17050 (2000).

37. J. J. Xiong, R. S. Phillips, D. M. Kurtz, S. Jin, J. Y. Ai, and J. Sanders-Loehr, The O-2 binding pocket of myohemerythrin: Role of a conserved leucine, *Biochemistry* **39,** 8526–8536 (2000).

38. S. J. Hubbard and J. M. Thornton, "NACCESS," computer program, Department of Biochemistry and Molecular Biology, University College London (1993).

39. D. L. Mattiello and R. Freeman, Blood, sweat, and tears. Toward a rehabilitation of the INADEQUATE experiment, *J. Magn. Reson.* **135,** 514–521 (1998).

40. M. Polak and G. Navon, Nuclear magnetic resonance studies of the interaction of molecular oxygen with organic compounds, *J. Phys. Chem.* **78,** 1747–1750 (1974).

41. K. Inoue, H. Yamada, T. Imoto, and K. Akasaka, High pressure NMR study of a small protein, gurmarin, *J. Biomol. NMR* **12,** 535–541 (1998).

42. R. Koradi, M. Billeter, and K. Wuthrich, MOLMOL: A program for display and analysis of macromolecular structures, *J. Mol. Graph.* **14,** 51-& (1996).